STIM2 targets Orai1/STIM1 to the AKAP79 signaling complex and confers coupling of Ca^{2+} entry with NFAT1 activation

Ga-Yeon Son[a,1], Krishna Prasad Subedi[a,2], Hwei Ling Ong[a,2], Lucile Noyer[b], Hassan Saadi[a], Changyu Zheng[c], Rajesh Bhardwaj[d], Stefan Feske[b], and Indu Suresh Ambudkar[a,3]

[a]Secretory Physiology Section, National Institute of Dental and Craniofacial Research, NIH, Bethesda, MD 20892; [b]Department of Pathology, New York University School of Medicine, New York, NY 10016; [c]Translational Research Core, National Institute of Dental and Craniofacial Research, NIH, Bethesda, MD 20892; and [d]Department of Nephrology and Hypertension, University Hospital Bern, Inselspital, 3010 Bern, Switzerland

Edited by Anjana Rao, La Jolla Institute for Allergy and Immunology, La Jolla, CA, and approved May 26, 2020 (received for review September 12, 2019)

The Orai1 channel is regulated by stromal interaction molecules STIM1 and STIM2 within endoplasmic reticulum (ER)-plasma membrane (PM) contact sites. Ca^{2+} signals generated by Orai1 activate Ca^{2+}-dependent gene expression. When compared with STIM1, STIM2 is a weak activator of Orai1, but it has been suggested to have a unique role in nuclear factor of activated T cells 1 (NFAT1) activation triggered by Orai1-mediated Ca^{2+} entry. In this study, we examined the contribution of STIM2 in NFAT1 activation. We report that STIM2 recruitment of Orai1/STIM1 to ER-PM junctions in response to depletion of ER-Ca^{2+} promotes assembly of the channel with AKAP79 to form a signaling complex that couples Orai1 channel function to the activation of NFAT1. Knockdown of STIM2 expression had relatively little effect on Orai1/STIM1 clustering or local and global $[Ca^{2+}]_i$ increases but significantly attenuated NFAT1 activation and assembly of Orai1 with AKAP79. STIM1ΔK, which lacks the PIP_2-binding polybasic domain, was recruited to ER-PM junctions following ER-Ca^{2+} depletion by binding to Orai1 and caused local and global $[Ca^{2+}]_i$ increases comparable to those induced by STIM1 activation of Orai1. However, in contrast to STIM1, STIM1ΔK induced less NFAT1 activation and attenuated the association of Orai1 with STIM2 and AKAP79. Orai1-AKAP79 interaction and NFAT1 activation were recovered by coexpressing STIM2 with STIM1ΔK. Replacing the PIP_2-binding domain of STIM1 with that of STIM2 eliminated the requirement of STIM2 for NFAT1 activation. Together, these data demonstrate an important role for STIM2 in coupling Orai1-mediated Ca^{2+} influx to NFAT1 activation.

STIM2 | NFAT1 | Orai1 | STIM1 | ER-PM junction

Store-operated calcium entry (SOCE), mediated by the plasma membrane (PM) channel Orai1, elicits specific cytosolic Ca^{2+} signals that are used by cells for regulating critical physiological processes, such as Ca^{2+}-dependent gene expression, cAMP generation, cell proliferation and migration, protein and fluid secretion, and inflammatory responses (1–3). SOCE is activated in response to depletion of Ca^{2+} within the endoplasmic reticulum (ER) lumen. Stromal interaction molecules (STIMs), STIM1 and STIM2, reside within the ER and sense decreases in $[Ca^{2+}]_{ER}$ via their luminal N-terminal Ca^{2+}-binding domains and undergo a conformational change that causes remodeling of the cytosolic C-terminal domains. As a consequence, STIMs multimerize and translocate to the cell periphery, where the PM and ER are tightly apposed, thereby enabling the interaction of their C-terminal polybasic domains with PM phosphatidylinositol 4,5-bisphosphate (PIP_2) (3, 4). This results in the formation of ER-PM junctions, where STIMs recruit and activate Orai1 channel via their STIM-Orai activating region (SOAR) domain (5–7).

Orai1-mediated Ca^{2+} entry generates distinct spatial and temporal Ca^{2+} signals. $[Ca^{2+}]_i$ increases close to the site of Ca^{2+} entry (local $[Ca^{2+}]_i$ increase) and in the bulk cytosol (global $[Ca^{2+}]_i$ increase) are sensed and decoded by different sensors and effector proteins (8). For example, local $[Ca^{2+}]_i$ elevation caused by Orai1 activity is reported as a major determinant in the activation of nuclear factor of activated T cells 1 (NFAT1), which is translocated to the nucleus, where it regulates Ca^{2+}-dependent gene expression (9). Furthermore, it has been shown that a sufficient increase in local $[Ca^{2+}]_i$ is achieved only when channels are clustered within ER-PM junctions (10), although there are contradictory data suggesting that Ca^{2+} entry via diffusely localized channels can also activate NFAT1 (11, 12). A strong coupling of Orai1 function with NFAT1 activation also depends on assembly of the channel with A-kinase anchoring protein 79 (AKAP79). This ensures that local Ca^{2+} entry mediated by the channel is sensed and used for activation of calcineurin, dephosphorylation of NFAT1, and translocation to the nucleus (13). Orai3, which has weak interaction with AKAP79 after store depletion, is also ineffective in activating NFAT1 (13).

STIM1 and STIM2 are the main proteins involved in clustering and activation of Orai1. STIM1 is the primary activator of

Significance

Ca^{2+} entry mediated by the plasma membrane (PM) channel Orai1 controls nuclear factor of activated T cells 1 (NFAT1)-dependent gene expression that regulates critical cellular functions. Ca^{2+}-sensing endoplasmic reticulum (ER) proteins, STIM1 and STIM2, regulate Orai1 function in response to decreases in $[Ca^{2+}]_{ER}$. While STIM1 is the primary regulator of Orai1 activity, STIM2 has a minor contribution to Ca^{2+} entry but is relevant for Ca^{2+}-dependent NFAT1 activation. Here we report that STIM2 recruits Orai1/STIM1 to ER-PM junctions and promotes channel assembly with the AKAP79 signaling complex. The latter is an important step that allows Ca^{2+} entry mediated by Orai1 to be specifically used for NFAT1 activation. Our findings reveal that STIM2 enhances the coupling of Orai1 function with NFAT1 activation.

Author contributions: G-Y.S., K.P.S., H.L.O., S.F., and I.S.A. designed research; G-Y.S., K.P.S., H.L.O., H.S., and C.Z. performed research; G-Y.S., K.P.S., H.L.O., L.N., C.Z., R.B., S.F., and I.S.A. contributed new reagents/analytic tools; G-Y.S., H.L.O., L.N., H.S., R.B., S.F., and I.S.A. analyzed data; and G-Y.S., K.P.S., H.L.O., H.S., R.B., S.F., and I.S.A. wrote the paper.

Competing interest statement: S.F. is a scientific cofounder of CalciMedica.

This article is a PNAS Direct Submission.

[1]Present address: Department of Molecular Pathobiology, New York University College of Dentistry, New York, NY, 10010.

[2]K.P.S. and H.L.O. contributed equally to this work.

[3]To whom correspondence may be addressed. Email: indu.ambudkar@nih.gov.

This article contains supporting information online at https://www.pnas.org/lookup/suppl/doi:10.1073/pnas.1915386117/-/DCSupplemental.

First published June 29, 2020.

Orai1, and loss of the protein eliminates Orai1 activation and, consequently, regulation of downstream Ca^{2+}-dependent cell functions. STIM1 clustering of Orai1 in ER-PM junctions is reported to strengthen the coupling of Orai1-mediated Ca^{2+} entry with NFAT1 activation (10). In contrast, activation of channels that are diffusely localized in the membrane by the cytosolic STIM1 C terminus or SOAR fragments has also been shown to induce nuclear translocation of NFAT1 and trigger gene expression in some studies (14–16). There is relatively less information about the role of STIM2 in regulating Orai1 function and Ca^{2+}-dependent gene expression. STIM2 induces weak activation of Orai1 and is suggested to regulate resting $[Ca^{2+}]_i$ in the cells (3, 17). Furthermore, owing to the relatively low Ca^{2+} affinity of its EF-hand domain, STIM2 can sense small decreases in $[Ca^{2+}]_{ER}$ (3). Our previous findings demonstrate that STIM2 modulates the cell response to low stimulus intensities by promoting recruitment of Orai1 and STIM1 to ER-PM junctions and facilitating STIM1 activation under conditions in which $[Ca^{2+}]_{ER}$ is not low enough to activate STIM1 (18, 19). Although STIM2 is not a major contributor to SOCE in most cell types, it appears to have a unique physiological relevance. Mice lacking the protein display developmental defects and die 4 to 6 wk after birth. In addition, differentiated T cells and T helper cells lacking STIM2 show small decreases in SOCE compared with STIM1-deficient cells that have almost a complete loss of SOCE. Despite the small decrease in SOCE, loss of STIM2 in these T cells causes a relatively large decrease in cytokine production that is attributed to a defect in nuclear translocation of NFAT1 (20). Up-regulation of STIM2 in pulmonary artery smooth muscle cells enhances NFAT signaling pathways to regulate cell proliferation (21). Moreover, in breast cancer cells, STIM2 is reported to have a specific role in NFAT1 regulation (22). While

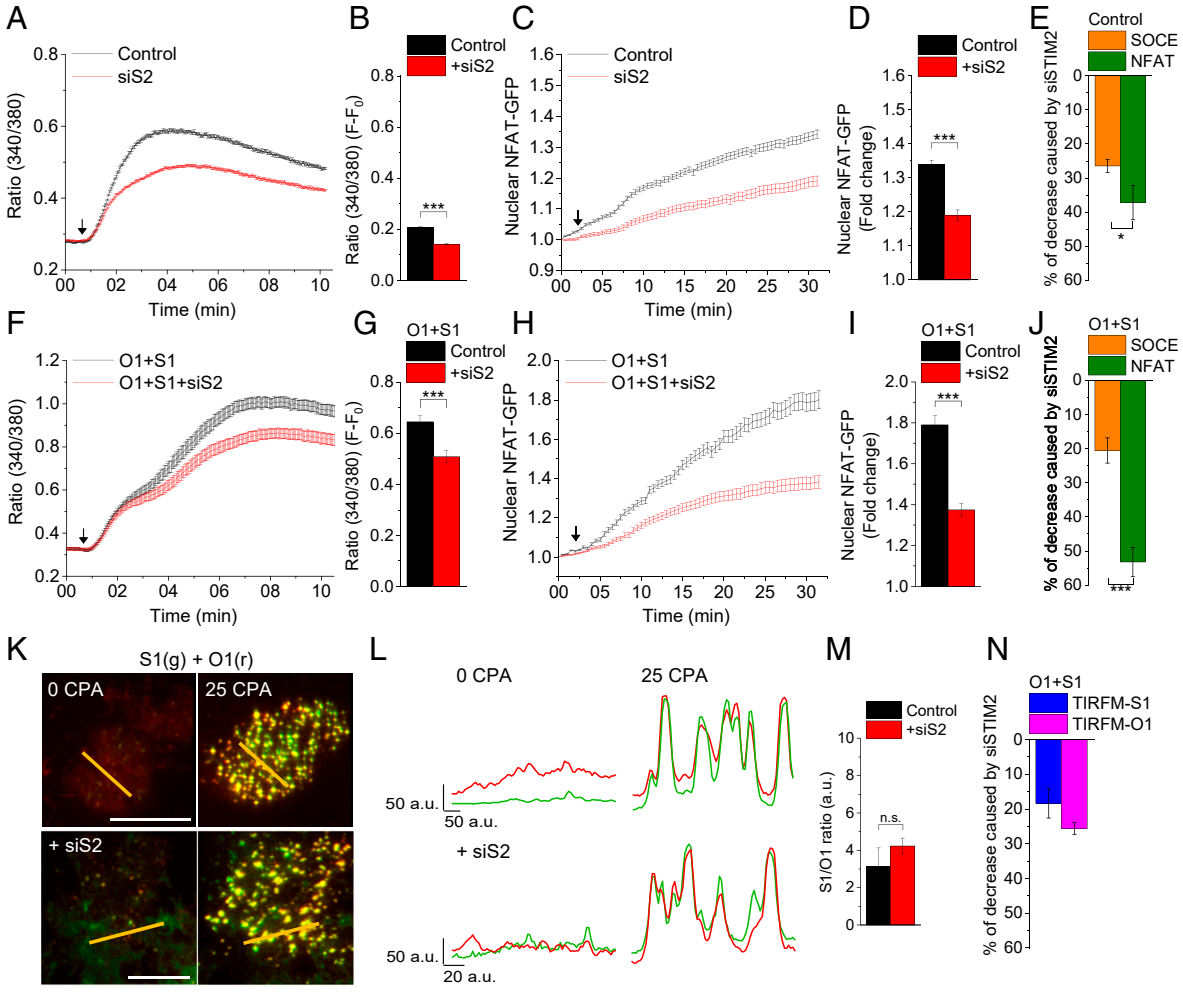

Fig. 1. Knockdown of STIM2 causes differential effects on SOCE and NFAT1 activation. Control (*A*–*E*) and Orai1+STIM1 (O1+S1)-expressing (*F*–*J*) HEK293 cells were treated with control siRNA (Control) or siSTIM2 (siS2) and used for measuring SOCE or nuclear translocation of NFAT1-GFP. (*A* and *F*) Time-dependent increase in Fura2 fluorescence (340/380-nm ratio) following stimulation with CPA. (*B* and *G*) Bar graphs showing the change in the 340/380 ratio at the 10-min time point ($F\text{-}F_0$). (*C* and *H*) Relative increase in nuclear NFAT1-GFP fluorescence in control and O1+S1 cells expressing NFAT1-GFP following stimulation with CPA. (*D* and *I*) Bar graphs showing nuclear NFAT1-GFP fluorescence at the 30-min time point. In all experiments, the addition of 25 μM CPA is indicated by an arrow in the graph. (*E* and *J*) Relative decreases in SOCE and nuclear import of NFAT1-GFP induced by siSTIM2 compared with their respective controls. (*K*) TIRFM images of Orai1-CFP (O1; red) and YFP-STIM1 (S1; green) in cells before and 10 min after 25 μM CPA stimulation (0 and 25 CPA, respectively). (Scale bar: 10 μm.) (*L*) Line scans through the image (position shown by orange line) showing clustering of the two proteins in unstimulated cells (*Left*) and stimulated cells (*Right*). (*M*) Bar graphs showing the STIM1:Orai1 fluorescence ratio in puncta in control and siSTIM2-treated cells. (*N*) Bar graph showing relative decreases of STIM1 and Orai1 signals in clusters induced by siSTIM2. Values are presented as mean ± SEM. Statistical tests were done using either Student's *t* tests for two groups or ANOVA with Sidak's multiple comparisons test for two or more groups. $*P < 0.05$, $***P < 0.001$; n.s., not significant ($P > 0.05$). For both the SOCE and NFAT experiments, the graphs show averaged data from 100 to 300 cells per group. For TIRFM images, images and line scans represent data from four experiments, while the bar graph shows averaged data of 30 to 60 cells.

the regulation of NFAT1 by Orai1/STIM1 has been studied extensively, there is not much information about the role of STIM2 in this process.

In the present study, we examined the contribution of STIM2 to the nuclear import of NFAT1 that is triggered in response to Orai1-mediated Ca^{2+} entry. We report that knockdown of STIM2 causes a large reduction in nuclear translocation of NFAT1 despite relatively small decreases in Orai1/STIM1 clustering within ER-PM junctions or global and local $[Ca^{2+}]_i$ increases. Our data reveal that assembly of Orai1/STIM1 with STIM2 in response to ER-Ca^{2+} depletion promotes the association of Orai1 with AKAP79 and enhances the nuclear translocation of NFAT1. In addition, we show that STIM1ΔK, a STIM1 mutant lacking the polybasic PIP_2-binding domain (amino acids 672 to 685), is recruited by Orai1 into ER-PM junctions, where it activates the channel to cause local and global $[Ca^{2+}]_i$ increases, which, although comparable to Orai1/STIM1, trigger relatively less NFAT1 activation. Further, neither STIM2 nor AKAP79 is assembled with the Orai1/STIM1ΔK complex. Importantly, expression of STIM2 with Orai1/STIM1ΔK restores the channel-AKAP79 interaction together with NFAT1 activation. A STIM1 chimera (STIM1-S2K) containing the STIM2-polybasic domain instead of its own not only causes clustering and activation of Orai1, but also eliminates the contribution of STIM2 in NFAT1 activation. Taken together, our findings demonstrate an important role for STIM2 in the recruitment of Orai1/STIM1 to ER-PM junctions, assembly of the channel with the AKAP79 signaling complex, and coupling of Ca^{2+} entry with activation of NFAT1.

Results

Differential Effects of STIM2 Knockdown on SOCE and NFAT1 Activation. Depletion of ER-Ca^{2+} in HEK293 cells using cyclopiazonic acid (CPA; 25 μM) induced a sustained elevation in $[Ca^{2+}]_i$, represented by an increase in Fura2-AM fluorescence at a 340/380 ratio. Knockdown of endogenous STIM2 expression by siSTIM2 reduced the $[Ca^{2+}]_i$ increase by approximately 25% compared with control cells treated with scrambled siRNA (Fig. 1 *A*, *B*, and *E*). Furthermore, a Ca^{2+} addback assay showed that Ca^{2+} influx, but not Ca^{2+} release from the ER, was reduced by siSTIM2 (*SI Appendix*, Fig. S1 *A* and *B*). Unless specified otherwise, all the experiments described below were carried out under the same conditions, in 25 μM CPA-stimulated HEK293 cells maintained in medium with 1 mM $CaCl_2$.

Next, we examined NFAT1 activation triggered by Orai1-mediated Ca^{2+} entry in response to depletion of ER-Ca^{2+}. CPA stimulation of cells resulted in activation of NFAT1, which was detected as a time-dependent increase in nuclear NFAT1-GFP (Fig. 1 *C* and *D*; bar graphs in *D* represent increase in nuclear NFAT1-GFP at the 30-min time point). Intriguingly, STIM2 knockdown induced a significantly greater decrease in nuclear accumulation of NFAT1 compared with the decrease in SOCE (Fig. 1*E*). Furthermore, the siSTIM2-induced decrease in nuclear import of NFAT1 was similar in cells stimulated with CPA and those stimulated with thapsigargin (Tg) (*SI Appendix*, Fig. S1 *C* and *D*; value at the 30-min time point is shown in the bar graphs). Our previous study (18) showed that knockdown of STIM2 causes a small, insignificant decrease in the percentage of cells showing nuclear NFAT at 10 min after stimulation with Tg; however, the time-dependent increase in nuclear NFAT1-GFP was not measured in that study. Since longer treatment with Tg causes significant changes in cell morphology, here we measured nuclear NFAT1-GFP and $[Ca^{2+}]_i$ changes in CPA-stimulated cells. We previously reported that knockdown of either Orai1 or STIM1 eliminates both SOCE and nuclear translocation of NFAT1 in HEK293 cells (18). Consistent with those findings, blocking channel function with Synta66 substantially reduced the nuclear translocation of NFAT1 (*SI Appendix*, Fig. S1 *E* and *F*; compare with nuclear NFAT level in unstimulated cells). While the inhibition by Synta66 does not conclusively rule out the contributions of Orai2 and Orai3 to NFAT1 activation, previous studies have shown that Orai1 is the major contributor to SOCE and NFAT1 activation in HEK293 cells (13). siSTIM2 decreased endogenous STIM2 protein expression but had no effect on endogenous STIM1 or Orai1 protein levels (*SI Appendix*, Fig. S1*G*).

The role of STIM2 in NFAT1 activation was further investigated in HEK293 cells overexpressing Orai1+STIM1. Expression of Orai1 and STIM1 induced an approximate threefold increase in SOCE (Fig. 1 *F* and *G*) and a twofold increase in NFAT1 translocation to the nucleus (Fig. 1 *H* and *I*) compared with that in control cells (Fig. 1 *A*–*D*). Knockdown of endogenous STIM2 in Orai1+STIM1-expressing cells caused a 20% decrease in SOCE (Fig. 1 *F*, *G*, and *J*). A similar decrease in Ca^{2+} entry was seen when a Ca^{2+} addback assay was used to measure SOCE in cells expressing Orai1+STIM1+siSTIM2 (*SI Appendix*, Fig. S1 *H* and *I*). However, knockdown of STIM2 caused a relatively large decrease (57%) in NFAT translocation in cells expressing Orai1+STIM1 (compare red trace with black trace in Fig. 1*H*). This decrease in NFAT1 translocation was significantly greater than the decrease in SOCE (Fig. 1*J*). These findings indicate that overexpression of Orai1+STIM1 cannot compensate for the reduction in NFAT1 activation caused by the knockdown of endogenous STIM2.

Clustering of Orai1 with STIM1 is reported to be a critical determinant of NFAT1 activation (8, 20, 23). We found robust coclustering of Orai1 and STIM1 following CPA stimulation of cells expressing Orai1+STIM1 with either scrambled siRNA or siSTIM2 (Fig. 1 *K* and *L*). Colocalization of Orai1 and STIM1 was not affected by STIM2 knockdown. For the images shown in Fig. 1*K*, Mander's colocalization coefficient values, measured using the ImageJ plugin EzColocalization (24), for Orai1 in control and siSTIM2-treated cells were 0.87 and 0.85, respectively. For STIM1, the coefficient values were 0.87 and 0.89, respectively, in the same cells.

To further evaluate the effect of STIM2 knockdown on clustering of Orai1 with STIM1, we measured the ratio of STIM1:-Orai1 fluorescence in individual puncta. Fig. 1*M* shows that STIM2 knockdown did not have a significant effect on the STIM1:Orai1 fluorescence ratio within each punctum. Consistent with the relatively small decrease in SOCE (Fig. 1 *F* and *G*), knockdown of endogenous STIM2 induced decreases of approximately 18% and 25% in the average fluorescence of STIM1 and Orai1, respectively (Fig. 1*N* and *SI Appendix*, Fig. S1*J*), compared with cells treated with scrambled siRNA.

Relevance of PM PIP_2 in Orai1/STIM1 Assembly and Function. PM PIP_2 within ER-PM junctions has an important role in the assembly of Orai1/STIM1 channels. Clustering of STIM proteins at ER-PM junctions, where they recruit and activate Orai1, is determined by their C-terminal polybasic, PIP_2-binding domain (15, 25). We used two different approaches to examine the role of PM PIP_2 in the assembly and function of Orai1/STIM1. The first approach involved depleting PM PIP_2 using a 5′-phosphatase that is recruited to the PM following rapamycin treatment (26). Cells with reduced PIP_2 (confirmed by measuring the PM association of PIP_2-binding marker Tubby (27) (*SI Appendix*, Fig. S2 *A* and *B*) displayed a 50% decrease in SOCE (Fig. 2 *A* and *B*; CPA was added 2 min after rapamycin addition), but not intracellular release (*SI Appendix*, Fig. S2 *C* and *D*). In contrast, accumulation of NFAT1 in the nucleus was reduced by 80% (Fig. 2 *C* and *D*). The relatively greater decrease in NFAT1 activation cannot be accounted for by the reduction in Orai1 and STIM1 clustering alone (37% and 50%, respectively) (*SI Appendix*, Fig. S2 *E* and *G*). Interestingly, the preclustering and

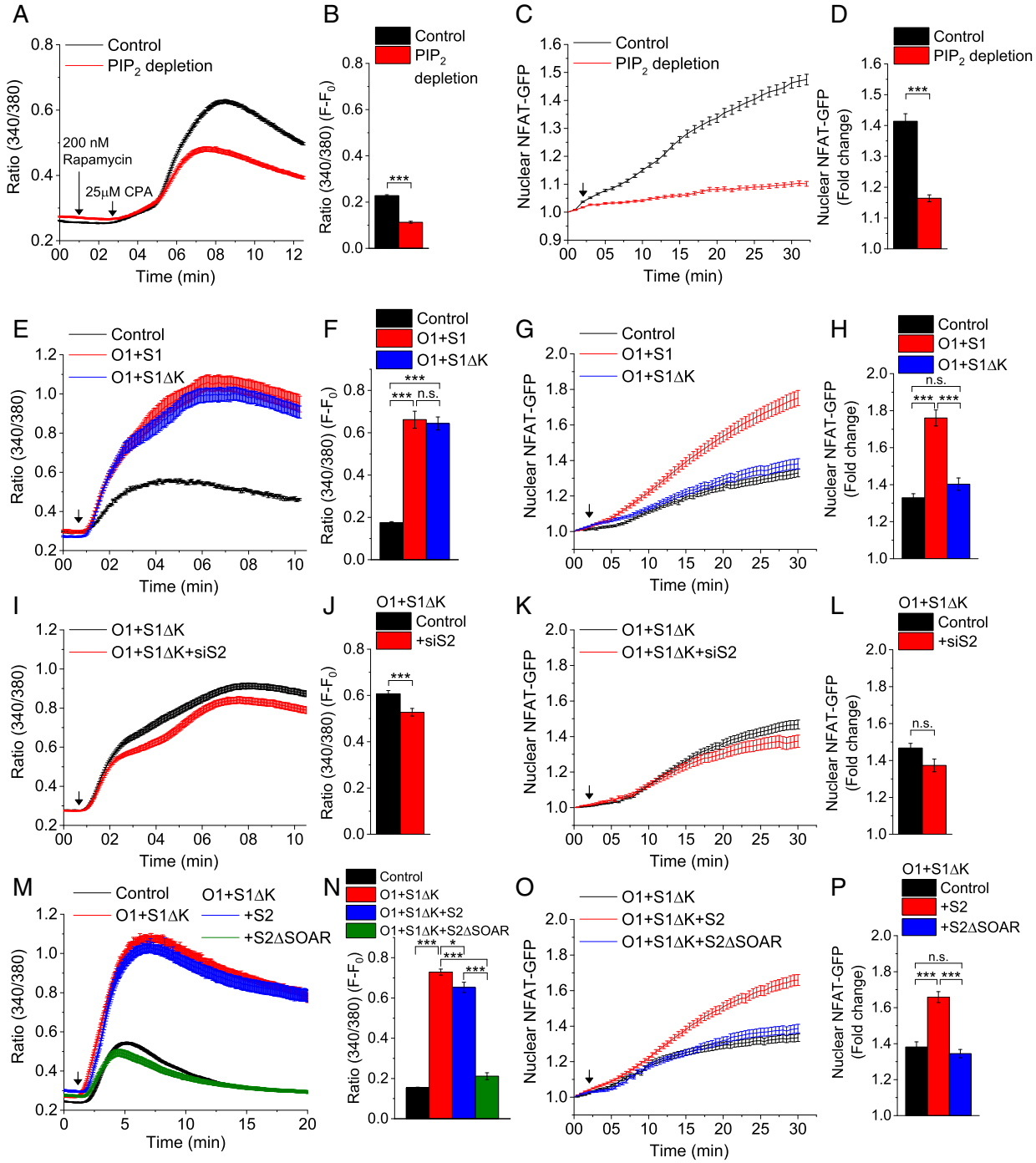

Fig. 2. Orai1+STIM1ΔK expression triggers SOCE but does not increase NFAT1 activation. (*A*) Time-dependent increase in the Fura2 fluorescence ratio (340/380) in control and PIP_2-depleted cells (with PIP_2 depletion triggered by adding rapamycin [first arrow] to cells expressing rapamycin-inducible 5′-phosphatase) following stimulation with CPA (second arrow). (*B*) Increase in the 340/380 ratio at the 10-min time point ($F\text{-}F_0$) in the control and PIP_2-depleted cells shown in *A*. (*C*) Relative increase in nuclear NFAT1-GFP in control and PIP_2-depleted cells. (*D*) Relative increase in nuclear NFAT1-GFP in control and PIP_2-depleted cells at the 30-min time point, calculated from data in *C*. (*E*) Fura2 fluorescence increase induced by CPA in control cells and cells expressing Orai1+STIM1 (O1+S1) or Orai1+STIM1ΔK (O1+S1ΔK). (*F*) Increase in the 340/380 ratio at the 10-min time point ($F\text{-}F_0$) in all three sets of cells shown in *E*. (*G*) Relative increase in nuclear NFAT1-GFP following CPA stimulation of control cells and cells expressing either O1+S1 or O1+S1ΔK. (*H*) Relative increase in nuclear NFAT1-GFP at the 30-min time point calculated from the data in *G*. (*I*) CPA-induced $[Ca^{2+}]_i$ increase in cells expressing O1+S1ΔK or O1+S1ΔK+siS2. (*J*) Increase in the 340/380 ratio at the 10-min time point ($F\text{-}F_0$) in O1+S1ΔK and O1+S1ΔK+siS2 cells. (*K*) Time-dependent increase in NFAT-GFP in the nucleus of cells expressing O1+S1ΔK or O1+S1ΔK+siS2. (*L*) Relative increase in nuclear NFAT1-GFP fluorescence at the 30-min time point. (*M*) Increase in the Fura2 fluorescence ratio in control cells and cells expressing O1+S1ΔK, O1+S1ΔK+S2, or O1+S1ΔK+S2ΔSOAR (S2ΔSOAR: STIM2 lacking the SOAR domain). (*N*) Increase in the 340/380 ratio at the 10-min time point ($F\text{-}F_0$) in all four sets of cells. (*O*) Relative increase in nuclear NFAT1-GFP fluorescence following CPA treatment of cells expressing O1+S1ΔK, O1+S1ΔK+S2, or O1+ S1ΔK+S2ΔSOAR. (*P*) Increase in nuclear NFAT1 at the 30-min time point. In all experiments, the addition of 25 μM CPA is indicated by an arrow on the graph. All values in the bar graphs are presented as mean ± SEM. Statistical tests were done using either Student's *t* test for two groups or ANOVA with Sidak's multiple comparisons test for two or more groups. $*P < 0.05$; $***P < 0.001$; n.s., not significant ($P > 0.05$). For both SOCE and NFAT experiments, the graphs show averaged data from 100 to 300 cells per group.

CPA-induced clustering of STIM2 was also decreased following depletion of PM PIP_2 (*SI Appendix*, Fig. S2 *F* and *G*).

In the second approach, we used STIM1ΔK, which lacks the PIP_2-binding domain and is unable to cluster in ER-PM junctions on its own even after ER-Ca^{2+} store depletion. When Orai1 is coexpressed, it can recruit STIM1ΔK by binding to its SOAR domain. Under these conditions, Orai1 and STIM1ΔK cocluster in puncta, and STIM1ΔK activates Orai1 to induce similar levels of channel activity as are achieved following STIM1 activation of the channel (15). CPA treatment of cells expressing either Orai1+STIM1 or Orai1+STIM1ΔK induced comparable increases in $[Ca^{2+}]_i$, approximately threefold over the level in control cells (Fig. 2 *E* and *F*). Similar to the data shown in Fig. 1 *C*, *D*, *H*, and *I*, cells expressing Orai1+STIM1 showed an almost twofold increase in nuclear NFAT1 compared with control cells (Fig. 2 *G* and *H*). Remarkably, in contrast to Orai1+STIM1, there was no significant enhancement of nuclear translocation of NFAT1 in cells expressing Orai1+STIM1ΔK

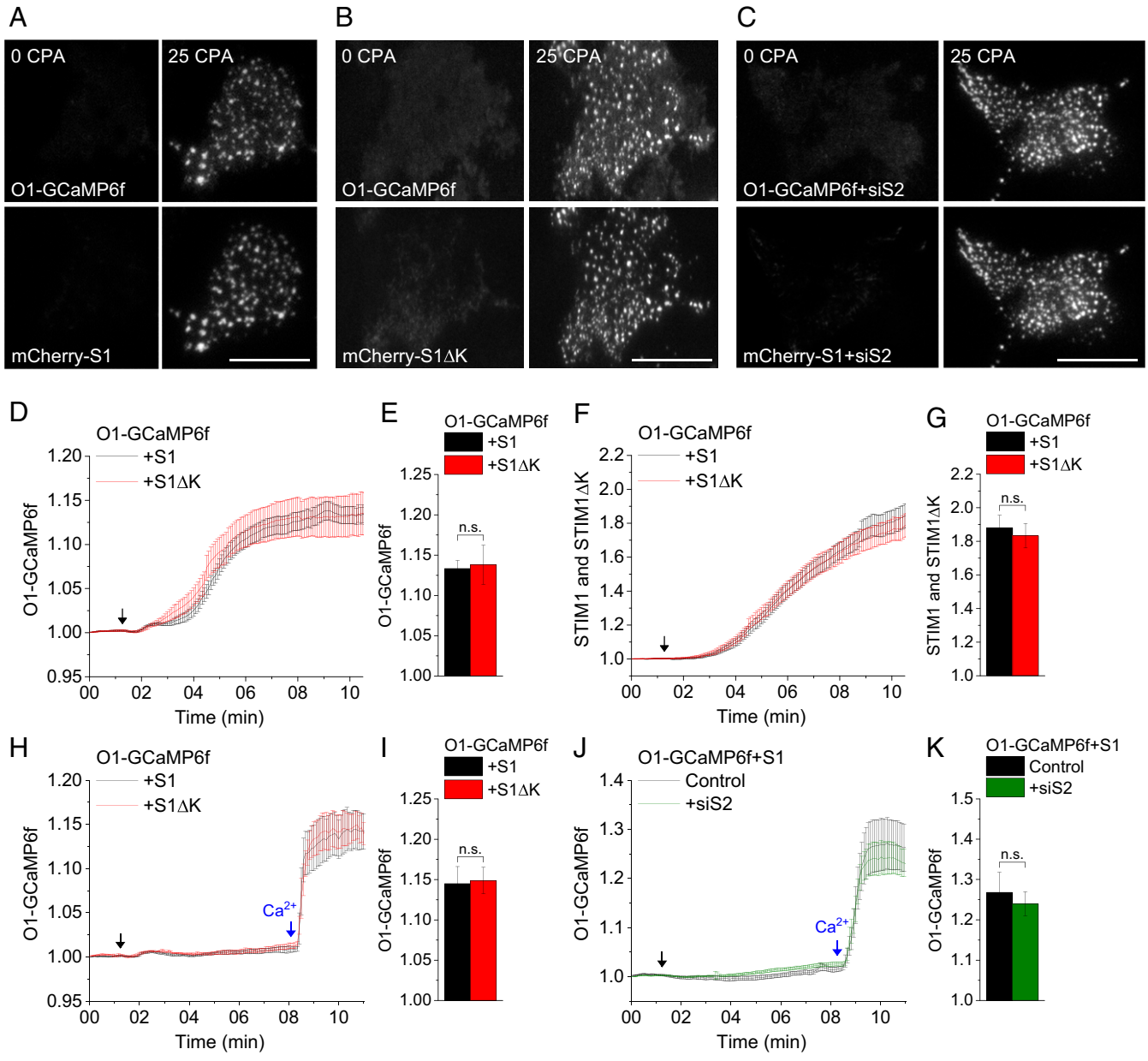

Fig. 3. Orai1+STIM1 and Orai1+STIM1ΔK induce similar increases in local $[Ca^{2+}]_i$. Orai1-GCaMP6f (O1-GCaMP6f) was coexpressed with either mCherry-tagged STIM1 (mCherry-S1) or STIM1ΔK (mCherry-S1ΔK). (*A*–*C*) TIRFM images of O1-GCaMP6f (*Upper*) coexpressed with mCherry-S1 (*Lower*) in control (*A*) and siSTIM2-treated (+siS2) (*C*) cells, or with mCherry-S1ΔK (*B*). Images were taken before and 10 min after stimulation with 25 μM CPA (0 and 25 CPA, respectively). (Scale bars: 10 μm.) (*D* and *E*) Time-dependent increase in O1-GCaMP6f puncta fluorescence (F/F_0) when coexpressed with either mCherry-S1 (S1) or mCherry-S1ΔK (S1ΔK). (*F* and *G*) Increases in mCherry-S1 (S1) or mCherry-S1ΔK (S1ΔK) fluorescence within O1-GCaMP6f puncta. For *D*–*G*, cells were stimulated with 25 μM CPA (arrows) in media containing 1 mM $CaCl_2$. (*H*–*K*) Ca^{2+}-addback experiments showing time-dependent increases in O1-GCaMP6f puncta fluorescence when coexpressed with either mCherry-S1 (S1) or mCherry-S1ΔK (S1ΔK) puncta (*H* and *I*) and with mCherry-S1 (S1) in control (Control) or siSTIM2-treated (+siS2) cells (*J* and *K*). Cells were first stimulated with 25 μM CPA in a nominally Ca^{2+}-free medium (black arrow), followed by 1 mM $CaCl_2$ (Ca^{2+}; blue arrow). All values in the bar graphs are presented as mean ± SEM and show the average fluorescence at the 10-min time point after stimulation. Statistical significance was assessed using Student's *t* test for two groups. n.s., not significant ($P > 0.05$). The TIRFM images represent data from three experiments, while the bar graph shows averaged data of 20 cells.

above that seen in control cells (Fig. 2 *G* and *H*). Since NFAT1 translocation to the nucleus is a relatively slow process, we also examined whether $[Ca^{2+}]_i$ elevation was sustained at later time points. Cells expressing either Orai1+STIM1 or Orai1+STIM1ΔK displayed similar kinetics of $[Ca^{2+}]_i$ elevation for up to 20 min after stimulation with CPA (*SI Appendix*, Fig. S2 *H* and *I*). These data indicate that the decrease of NFAT1 activation in Orai1+STIM1ΔK-expressing cells likely is not due to a reduction of SOCE.

Possible differences in clustering of wild-type or mutant STIM1 with Orai1 were examined using total internal reflection fluorescence microscopy (TIRFM). In response to CPA treatment, STIM1 aggregated in clusters at ER-PM junctions (*SI Appendix*, Fig. S3*A*). When the ER marker protein mCherry-ER3 was coexpressed with Orai1 and STIM1, all three were detected within the same puncta (*SI Appendix*, Fig. S3*B*; the increase in the mCherry signal likely represents ER that is closer to the PM within the junctions). In contrast to wild-type STIM1, STIM1ΔK did not cluster in ER-PM junctions after store depletion when expressed alone (*SI Appendix*, Fig. S3*C*). Coexpression of Orai1 rescued the clustering of STIM1ΔK following CPA stimulation, and both proteins coclustered with the ER marker protein (*SI Appendix*, Fig. S3*D*). The relative increases in puncta intensity for either STIM1 or STIM1ΔK and coexpressed Orai1 were similar (*SI Appendix*, Fig. S3*E*).

STIM2 Rescues NFAT Activation in Cells Expressing Orai1/STIM1ΔK without Affecting Ca^{2+} Entry. The findings reported above suggest that coexpression of Orai1+STIM1ΔK mediates SOCE as efficiently as coexpression of Orai1+STIM1. Despite this, nuclear translocation of NFAT1 was greatly reduced in the case of Orai1+STIM1ΔK. Interestingly, knockdown of STIM2 in Orai1+STIM1ΔK-expressing cells caused a small decrease in SOCE but no significant change in NFAT1 activation (Fig. 2 *I*–*L*), in contrast to the relatively large decrease in NFAT1 activation due to STIM2 knockdown in Orai1+STIM1-expressing cells (Fig. 1 *F*–*J*). These data indicate a key difference between the requirements of Orai1/STIM1ΔK and of Orai1/STIM1 for STIM2 in NFAT1 activation.

It is important to note that STIM1ΔK is recruited to ER-PM junctions by interacting with Orai1 via its SOAR domain, while full-length STIM1 is recruited to the junctions via binding of its polybasic domain to PM PIP_2. Consistent with findings reported in our previous study (18), STIM1ΔK was recruited into ER-PM junctions when expressed with STIM2 (junctions defined by mCherry-ER3, which was coexpressed with STIM proteins) (*SI Appendix*, Fig. S3 *F* and *H*). When Orai1 was coexpressed, all three proteins coclustered within the junctions (*SI Appendix*, Fig. S3 *G* and *H*). Coexpression of STIM2 caused a small but significant decrease in the $[Ca^{2+}]_i$ elevation in cells expressing Orai1+STIM1ΔK (Fig. 2 *M* and *N*) compared with cells not expressing STIM2 (Fig. 2 *E* and *F*). In contrast, STIM2 coexpression caused a marked recovery of NFAT1 nuclear translocation in cells expressing Orai1+STIM1ΔK to levels comparable to those in cells expressing Orai1+STIM1 (Fig. 2 *O* and *P*; compare Fig. 1 *H* and *I*). The SOAR domains of STIM1 and STIM2 mediate the interaction of both STIMs with Orai1, as well as with each other (2, 19). When STIM2ΔSOAR (which lacks the SOAR domain) was expressed together with Orai1+STIM1ΔK, there was no enhancement of NFAT1 activation, in contrast to the recovery induced by expression of STIM2 (Fig. 2 *O* and *P*). This suggests that the STIM2-SOAR domain is required for the regulation of NFAT1 activation by STIM2. Of note, although coexpression of STIM2 with Orai1+STIM1 did not enhance either CPA-induced SOCE or nuclear translocation of NFAT1 (*SI Appendix*, Fig. S3 *I*–*L*), coexpression of STIM2ΔSOAR with Orai1+STIM1 suppressed both SOCE and NFAT activation (Fig. 2 *M*–*P*). This finding is consistent with the reported dominant negative effect of STIM2ΔSOAR on SOCE (19).

Orai1/STIM1ΔK and Orai1/STIM1 Mediate Similar Increases in Local $[Ca^{2+}]_i$. Local $[Ca^{2+}]_i$ close to the site of Ca^{2+} entry is reported to be a primary determinant of NFAT1 activation (28). To determine whether variations in Orai1-mediated increases of local $[Ca^{2+}]_i$ in cells expressing Orai1+STIM1 or Orai1+STIM1ΔK account for the differences in NFAT1 activation, we expressed Orai1-GCaMP6f with the respective STIM proteins. Fusion of the calcium sensor GCaMP6f to Orai1 allows detection of local $[Ca^{2+}]_i$ increases near the channel pores (29). TIRFM images acquired before and after stimulation with CPA showed that Orai1-GCaMP6f displayed similar clustering patterns as STIM1 and STIM1ΔK (Fig. 3 *A* and *B*). The clustering of Orai1/STIM1 and fluorescence intensities of Orai1-GCaMP6f and STIM1 within the puncta were unaffected by siSTIM2 treatment (Fig. 3*C*). Importantly, the fluorescence intensity of Orai1-GCaMP6f following stimulation with CPA was detected primarily in clusters that coincided with STIM1 puncta, consistent with the activation of Orai1 within STIM1 clusters (Fig. 3 *D*–*G*).

To further confirm this readout, we measured Orai1-GCaMP6f fluorescence in cells coexpressing either STIM1 or STIM1ΔK using a Ca^{2+} addback assay. There was no increase in Orai1-GCaMP6f fluorescence during treatment with CPA in a Ca^{2+}-free medium, suggesting that the reporter does not detect $[Ca^{2+}]_i$ changes due to Ca^{2+} release from ER stores. However, when external Ca^{2+} was restored, there was a sharp increase in the Orai1-GCaMP6f signal (Fig. 3 *H* and *I*). This increase was similar in both sets of cells and represents the change in local $[Ca^{2+}]_i$ due to Orai1-mediated Ca^{2+} entry. Using a similar approach, we measured the effect of STIM2 knockdown on local $[Ca^{2+}]_i$ mediated by Orai1-GCaMP6f+STIM1. Similar increases in local $[Ca^{2+}]_i$ were detected in siSTIM2-treated and control cells, suggesting that knockdown of endogenous STIM2 did not affect the local $[Ca^{2+}]_i$ increase (Fig. 3 *J* and *K*). Therefore, we exclude the possibility that alterations in local $[Ca^{2+}]_i$ account for impaired activation of NFAT1 in cells with knockdown of STIM2 expression. In addition, the data presented in Fig. 1 show that the decrease in global $[Ca^{2+}]_i$ induced by STIM2 knockdown is relatively small and cannot account for the larger decrease in NFAT1 activation.

STIM2 Promotes Interaction of Orai1 with AKAP79. Clustering of Orai1 in ER-PM junctions in response to depletion of ER-Ca^{2+} stores promotes the interaction of Orai1 with AKAP79 and calcineurin, which localizes the Ca^{2+}-dependent phosphatase close to the site of Ca^{2+} entry (13). The role of AKAP79 in coupling local Ca^{2+} entry with NFAT1 activation was first described for L-type Ca^{2+} channels in neuronal cells (30). We examined the contribution of STIM2 to Orai1-AKAP79 association. Knockdown of endogenous AKAP79 did not affect the CPA-stimulated $[Ca^{2+}]_i$ increase in HEK293 cells but significantly reduced the nuclear translocation of NFAT1, by approximately 50% (Fig. 4 *A*–*D*; reduction of endogenous AKAP79 protein by siAKAP79 shown in Fig. 4*E*). Consistent with previous reports (13, 31), ER-Ca^{2+} store depletion increased the association of AKAP79 with Orai1 as determined by coimmunoprecipitation (co-IP) (Fig. 4 *F* and *G*). Importantly, knockdown of endogenous STIM2 abrogated the store-dependent increase in Orai1-AKAP79 association (Fig. 4 *F* and *G*).

Assembly of the Orai1-AKAP79 complex was examined in HEK293 cells expressing Orai1+STIM1, which display a CPA-induced increase in $[Ca^{2+}]_i$ and nuclear import of NFAT1, or cells expressing Orai1+STIM1ΔK, which display a CPA-induced increase in $[Ca^{2+}]_i$ but relatively less nuclear import of NFAT1. A 50% enhancement of the association between Orai1 and endogenous AKAP79 was seen following ER-Ca^{2+} store depletion in cells expressing Orai1+STIM1, which was not detected in cells expressing Orai1+STIM1ΔK. Western blot analysis showed co-IP of Myc-Orai1 and endogenous AKAP79 (Fig. 4 *H* and *I*). These findings indicate that the Orai1-STIM1ΔK complex interacts poorly with AKAP79 following Ca^{2+} store depletion,

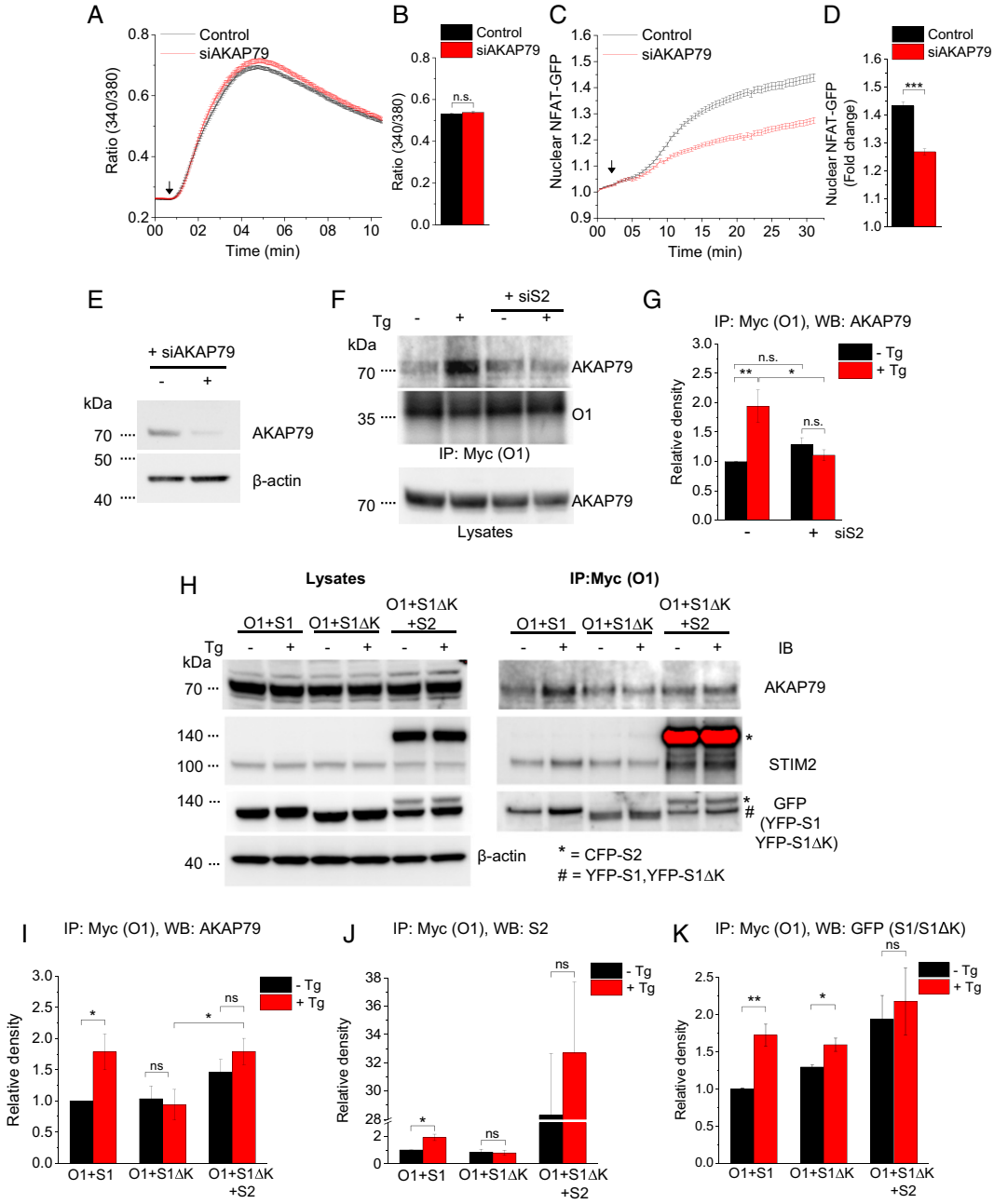

Fig. 4. Involvement of STIM2 in Orai1-AKAP79 interaction. (*A*) Fura2 fluorescence ratio (340/380) in control cells and cells treated with siAKAP79 stimulated with 25 μM CPA (arrow). (*B*) Bar graph showing averaged 340/380 ratio at the 10-min time point from three experiments. (*C*) Relative increase in nuclear NFAT1-GFP fluorescence following stimulation with 25 μM CPA (arrow) in control cells and cells treated with siAKAP79. (*D*) Bar graphs showing nuclear fluorescence values at the 30-min time point. All values in the bar graphs are presented as mean ± SEM. (*E*) Western blots showing AKAP79 protein in cells treated with control siRNA and siAKAP79, representative of data from three experiments. (*F*) Western blots showing co-IP of AKAP79 with Myc-Orai1 (O1) and AKAP79 in lysates (used as a loading control). Samples were obtained from control and siSTIM2-treated (siS2) cells, either unstimulated or at 5 min after stimulation with 1 μM Tg. Antibodies against Orai1 (O1; 1:1,000) and AKAP79 (1:1,000) were used. Data are representative of three experiments. (*G*) Bar graph showing the average density of AKAP79 in IP fractions. AKAP79 protein density was normalized to its loading control in the lysate and is expressed relative to that in unstimulated Orai1-expressing cells. Data were obtained from Western blots of three experiments. (*H*, *Right*) Western blots showing co-IP of AKAP79 (*Top*), STIM2 (S2; *Middle*) and STIM1 or STIM1ΔK (S1 or S1ΔK; *Bottom*) with Myc-Orai1. Samples were obtained from unstimulated cells or Tg-stimulated (at 5 min after stimulation) cells expressing Myc-Orai1+YFP-STIM1 (O1+S1), Myc-Orai1+YFP-STIM1ΔK (O1+S1ΔK), or Myc-Orai1+YFP-STIM1ΔK+CFP-STIM2 (O1+S1ΔK+S2). IP was performed using anti-Myc magnetic beads, with immunoblotting (IB) antibodies anti-AKAP79 and anti-STIM2 (1:1,000), anti-GFP (1:1,000), and β-actin (1:5,000). Note that the anti-STIM2 antibody detected both endogenous (S2) and expressed (CFP-S2) in the O1+S1ΔK+S2 lanes, while the anti-GFP antibody detected YFP- STIM1, YFP- STIM1ΔK, and CFP-STIM2. (*H*, *Left*) Western blots of the protein loading controls for AKAP79, STIM2, STIM1, STIM1ΔK, and β-actin in the lysates of all samples. Blots showing endogenous STIM2, detected using anti-STIM2 antibody, were exposed for longer periods. The red color in the blot indicates saturated pixels. (*I–K*) Bar graphs showing the averaged densities of AKAP79, STIM2, and STIM1 (wild type in lanes 1 and 2; STIM1ΔK in lanes 3 to 6) from four experiments. In each case, protein level was first normalized to its respective loading control and then expressed relative to the value in unstimulated Orai1+STIM1- expressing cells. All values in the bar graphs are presented as mean ± SEM. Statistical tests were done using either Student's *t* test for two groups or ANOVA with Sidak's multiple comparisons test for two or more groups (*G* and *I*). $*P < 0.05$; $**P < 0.01$; $***P < 0.001$; n.s., not significant ($P > 0.05$).

which could account for the reduced NFAT1 activation described above.

We next tested the role of STIM2 in the formation of Orai1-STIM1-AKAP79 complexes. Orai1+STIM1, but not Orai1+STIM1ΔK, displayed increased association with endogenous STIM2 in response to ER-Ca^{2+} store depletion. (Co-IP of Myc-Orai1 with endogenous STIM2 is shown in Fig. 4 *H* and *J*.) Furthermore, ER-Ca^{2+} store depletion enhanced the Orai1+STIM1 and Orai1+STIM1ΔK associations. (Co-IP of Myc-Orai1 with these STIM1 proteins is shown in Fig. 4 *H* and *K*.)

To further demonstrate the role of STIM2 in the coupling of Orai1 function to NFAT1 activation, we coexpressed STIM2 with Orai1+STIM1ΔK. The Orai1-AKAP79 association was higher in cells expressing Orai1+STIM1ΔK+STIM2 compared with cells expressing only Orai1+STIM1ΔK. (Co-IP of Myc-Orai1 with endogenous AKAP79 is shown in Fig. 4 *H* and *I*.) The Orai1-AKAP79 association in the presence of STIM2 was increased even under resting conditions and did not increase significantly after ER store depletion. These data demonstrate that coexpression of STIM2 with Orai1+STIM1ΔK promotes the assembly of a complex containing STIM2, STIM1ΔK, Orai1, and AKAP79 even without ER-Ca^{2+} depletion (Fig. 4 *H*, *J*, and *K*). AKAP79 recruitment is mediated by Orai1, since knockdown of Orai1 abrogated the co-IP of AKAP79 with STIM2 (*SI Appendix*, Fig. S3*M*).

STIM2 Polybasic Domain Targets Orai1+STIM1 to ER-PM Junctions and Enhances Association with AKAP79. The polybasic domains of STIM1 and STIM2 critically determine the targeting of both proteins to ER-PM junctions. The STIM2 polybasic domain exerts a dominant effect on the function and assembly of the protein in ER-PM junctions, since deletion of the domain abolishes its clustering in ER-PM junctions. In contrast to STIM1ΔK, the clustering of STIM2ΔK is not rescued by coexpression of Orai1 (18). Therefore, we assessed the role of the STIM2 polybasic domain in recruiting Orai1 and STIM1 to ER-PM junctions and promoting their interaction with AKAP79. Toward this end, we used a chimeric construct of STIM1 in which its C-terminal polybasic domain was replaced with that of STIM2 (STIM1-S2K). ER-Ca^{2+} store depletion in cells expressing Orai1+STIM1-S2K resulted in a $[Ca^{2+}]_i$ increase comparable to that seen in cells expressing Orai1+STIM1 (Fig. 5 *A* and *B*). Knockdown of STIM2 expression in Orai1+STIM1-S2K cells did not reduce SOCE, in contrast to cells expressing Orai1+STIM1. The store depletion-induced nuclear translocation of NFAT1 in cells expressing Orai1+STIM1-S2K was also similar to that in cells expressing Orai1+STIM1 (Fig. 5 *C* and *D*). Importantly, knockdown of endogenous STIM2 in cells expressing Orai1+STIM1-S2K did not impair the nuclear translocation of NFAT1 (Fig. 5 *E* and *F*), unlike in cells expressing Orai1+STIM1 (Fig. 1 *H* and *I*), in which a 60% decrease was observed. The analysis of STIM1-S2K localization by TIRFM revealed that it was preclustered in ER-PM junctions even before store depletion (Fig. 5*G*), as previously reported for STIM2 (3, 18, 19). Store depletion further enhanced the clustering of STIM1-S2K (Fig. 5*G*). STIM1-S2K also colocalized with Orai1 in puncta in unstimulated cells, and this coclustering was enhanced by CPA-mediated store depletion (Fig. 5*H*).

Discussion

Herein we describe a distinct role for STIM2 in regulating NFAT1 activation that is triggered by Orai1-mediated Ca^{2+} entry. Our findings establish that STIM2-mediated targeting of Orai1 and STIM1 to ER-PM junctions promotes assembly of the channel with the AKAP79/calcineurin signaling complex and strengthens the coupling of channel function to NFAT1 activation. As reported previously, the association of Orai1 with AKAP79 allows for the selective use of local $[Ca^{2+}]_i$ increases evoked by Orai1 for activation of calcineurin, which then leads to dephosphorylation of NFAT1 and translocation into the nucleus (13). We show that decreasing the expression of endogenous STIM2 attenuates the Orai1-AKAP79 interaction and causes a substantial reduction in NFAT1 activation but only minor decreases in Ca^{2+} entry and Orai1/STIM1 clustering. Taken together, these findings suggest that under conditions in which ER-Ca^{2+} stores are maximally depleted, STIM1 has the major role in clustering and activating Orai1, whereas STIM2 contributes to the efficiency of Orai1-dependent NFAT1 activation. Importantly, the significant decrease in NFAT1 activation caused by STIM2 knockdown is not due to attenuation of local or global $[Ca^{2+}]_i$ increases resulting from Orai1-mediated Ca^{2+} entry. We show that $[Ca^{2+}]_i$ increases primarily on clustering of Orai1 and STIM1 and activation of the channel within ER-PM junctions. However, coupling of Orai1-mediated Ca^{2+} influx to NFAT1 activation is dependent on the assembly of Orai1 with AKAP79, which is determined by STIM2 that targets Orai1 and STIM1 to the AKAP79 signaling complex.

We have provided further evidence for the role of STIM2 in coupling Orai1 channel function and NFAT activation by using a STIM1 mutant, STIM1ΔK, which lacks the PIP_2-binding domain and does not form puncta on its own. STIM1ΔK is recruited by Orai1 to cluster in ER-PM junctions, where it activates the channel and causes local and global $[Ca^{2+}]_i$ increases comparable to those in cells expressing Orai1 and STIM1. However, NFAT1 activation in cells expressing STIM1ΔK is strongly reduced compared with that in cells expressing Orai1+STIM1. A key finding of this study is that coexpression of STIM2 with Orai1/STIM1ΔK leads to coclustering of all three proteins, interaction of Orai1 with AKAP79, and recovery of NFAT1 activation. We further demonstrate the relevance of the STIM2-polybasic domain in assembly of the Orai1-AKAP79 signaling complex by substituting the STIM1-polybasic domain with that of STIM2 (STIM1-S2K). Interestingly, NFAT activation induced by Orai1/STIM1-S2K, unlike Orai1/STIM1, is not dependent on endogenous STIM2. The STIM2-polybasic domain has been shown to have a stronger affinity for PM PIP_2 compared with the STIM1-polybasic domain (25, 32), which might determine how STIM2 regulates the assembly of STIM1 and Orai1 with AKAP79. Taken together, our findings support a specific role for STIM2 in targeting Orai1/STIM1 to ER-PM junctions and the coupling of channel function to NFAT1 activation (interaction 1 in the model presented in Fig. 6). However, our findings do not rule out the possibility that STIM2 might exert a functionally relevant effect on the organization of ER-PM junctions that secondarily favors an Orai1-AKAP79 interaction and increases the efficiency of Orai1-NFAT1 coupling (interaction 2 in Fig. 6). Further studies are needed to elucidate the effect of STIM2 on ER-PM junctions.

The data we present here reveal a possible mechanism by which STIM2 regulates NFAT1 signaling. We hypothesize that STIM2 recruits Orai1/STIM1 to ER-PM junctions to promote assembly of the channel with the AKAP79/calcineurin signaling complex. This enhances the coupling of Ca^{2+} influx with activation of NFAT1. We previously showed that STIM2 can detect relatively small changes in $[Ca^{2+}]_{ER}$ and increase Orai1/STIM1 function in cells treated with low-intensity stimuli (18). This augmentation of SOCE is due to an STIM2-dependent increase in the clustering of Orai1/STIM1 at relatively low [agonist], which does not induce a sufficient decrease in $[Ca^{2+}]_{ER}$ to elicit a STIM1 response. We further established that in cells with minimal depletion of ER-Ca^{2+} stores, STIM2 can recruit STIM1 and trigger remodeling of the STIM1 C terminus to cause Orai1/STIM1 coupling and channel activation (19). These previous findings cannot explain the role of STIM2 in coupling Orai1 function with NFAT activation that we have described above. In the present study, cells were stimulated to induce maximal depletion of ER-Ca^{2+}. Under these conditions, STIM1 is fully

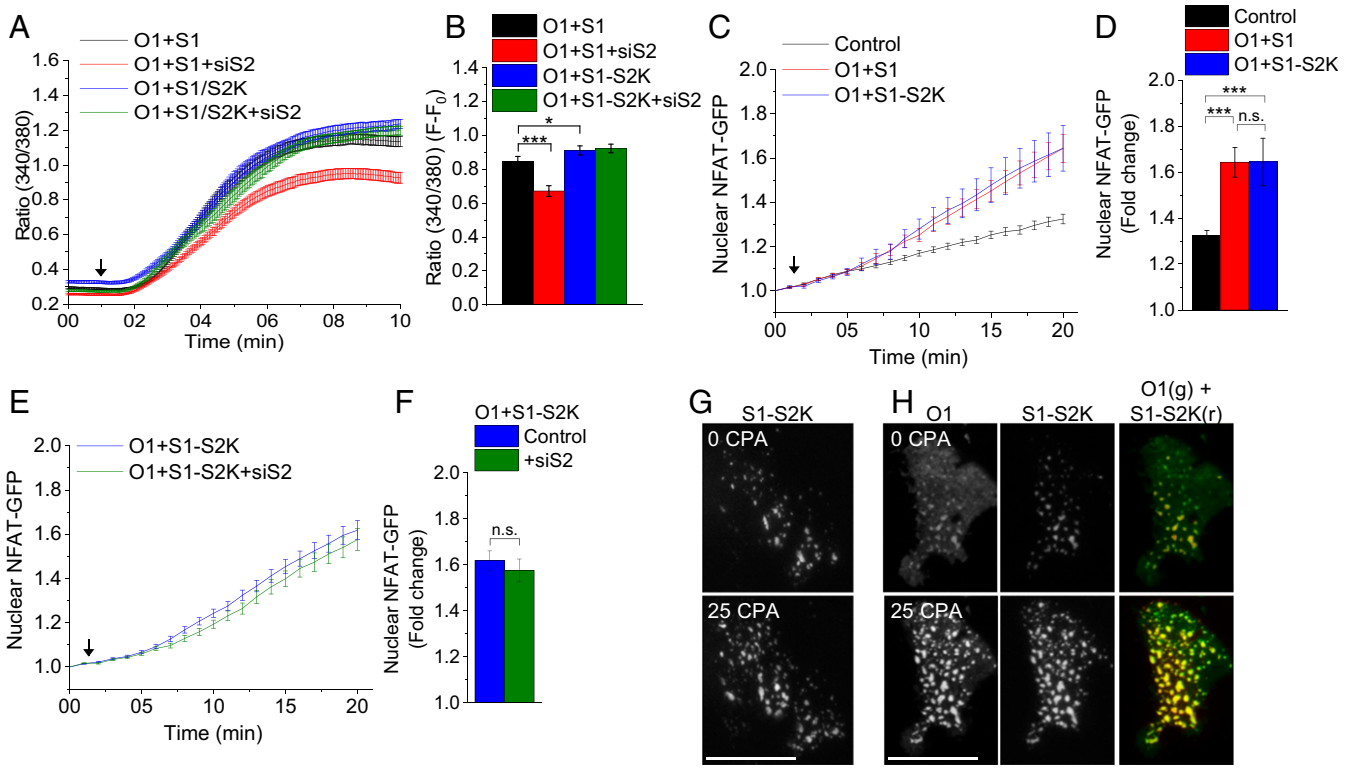

Fig. 5. The STIM2 polybasic domain targets Orai1/STIM1 to ER-PM junctions accessible to the AKAP signaling complex. (*A*) Fura2 fluorescence in CPA-treated cells expressing Orai1+STIM1 (O1+S1) and Orai1+STIM1-S2K (O1+S1-S2K), with and without siSTIM2 treatment (O1+S1+siS2, O1+S1-S2K+siS2). (*B*) Increase in the 340/380 ratio ($F-F_0$) at the 10-min time point in all four sets of cells. (*C*) Relative increase in nuclear NFAT1-GFP following CPA treatment of control cells and cells expressing O1+S1 and O1+S1-S2K. (*D*) Increase in nuclear NFAT1-GFP fluorescence at the 20-min time point. (*E*) Relative increase in nuclear NFAT1-GFP following CPA treatment of control cells and cells expressing O1+S1-S2K and O1+S1-S2K+siS2. (*F*) Relative changes in NFAT1-GFP fluorescence at the 20-min time point. (*G*) TIRFM images of mCherry-STIM1-S2K (S1-S2K) in resting and CPA-stimulated cells at the 10-min time point. (*H*) TIRFM images of Orai1-CFP (O1) and S1-S2K in resting and CPA-stimulated cells at the 10-min time point. In all experiments, the addition of 25 μM CPA is indicated by an arrow. All values in the bar graphs are presented as mean ± SEM. Statistical tests were done using either Student's *t* test for two groups or ANOVA with Sidak's multiple comparisons test for two or more groups. $*P < 0.05$; $***P < 0.001$; n.s., not significant ($P > 0.05$). For both SOCE and NFAT experiments, the graphs show averaged data from 100 to 300 cells per group. For TIRFM experiments, the images show representative cells from four experiments.

mobilized and has a dominant role in Orai1 clustering and activation; however, STIM2, but not STIM1, has a more significant role in NFAT1 activation triggered by Orai1-mediated Ca^{2+} entry. Therefore, our findings suggest that in addition to enhancing SOCE at low stimulus intensities, STIM2 promotes the assembly of Orai1 with the AKAP79 signaling complex, which is a key step in triggering the nuclear transport of NFAT1. STIM2 strengthens the coupling of Orai1 channel function with NFAT1 activation, even though STIM1 is sufficient for clustering and activating Orai1 to cause a sufficient increase in local $[Ca^{2+}]_i$.

AKAP79 is a prototypical protein kinase A (PKA) anchoring protein that directly interacts with several receptors, ion channels, and adenylyl cyclases (33–36). Interestingly, Ca^{2+} entry via Orai1 also triggers the activation of adenylyl cyclase 8 (AC8) within ER-PM junctions (37, 38). Thus, assembly of Orai1 with the AKAP79 signaling complex facilitates the activation of NFAT1- and cAMP-dependent signaling pathways, both of which are critical for cell function and regulation of gene expression. An additional role for the locally generated cAMP in regulation of Orai1 function has been reported recently (31). In that study, AKAP79 was preferentially associated with Orai1 and required for PKA-mediated fast Ca^{2+}-dependent inactivation of the channel. Although further studies are needed to establish whether STIM2 is required for SOCE-dependent AC8 activation, we can hypothesize that STIM2 targeting of Orai1 to the AKAP79 complex could also control fast Ca^{2+}-dependent inactivation of the channel. Thus, STIM2 may exert bifunctional effects on the regulation of Orai1 channel activity: enhancing the function at low stimulus intensities by promoting Orai1/STIM1 clustering and STIM1 activation (18, 19), while controlling cAMP-dependent fast inactivation of Orai1 at high stimulus intensities when the channel is maximally activated. Further studies are needed to conclusively establish the physiological relevance of STIM2-dependent modulation of NFAT1 activation.

In conclusion, our findings demonstrate that STIM2 targets Orai1/STIM1 to ER-PM junctions to promote assembly of Orai1 with the AKAP79 signaling complex, which is an important determinant in coupling channel function with the activation of NFAT1. Thus, although STIM2 causes relatively weak activation of Orai1, it determines the efficiency of cells in using Orai1-generated $[Ca^{2+}]_i$ signals for regulation of NFAT1 signaling.

Materials and Methods

Cell Culture and Transfection. HEK293 cells were maintained in DMEM containing 10% heat-inactivated FBS, 1% glutamine, and 1% penicillin/streptomycin (Life Technologies) at 37 °C in 5% CO_2. Cells were transfected with plasmids using Lipofectamine 2000 (Life Technologies) or small interfering RNAs (siRNAs) using Lipofectamine RNAiMAX (Life Technologies). Transfected cells were maintained in Opti-MEM medium (Life Technologies) for 2 to 5 h and then in cell culture medium. Control cells were transfected with empty vector or a scrambled siRNA. Cells were typically used at 24 to 48 h after transfection. siAKAP79 and siOrai1 were obtained from Dharmacon, and siSTIM2 was from Life Technologies. All other reagents used were of molecular biology grade and were obtained from Sigma-Aldrich unless noted otherwise.

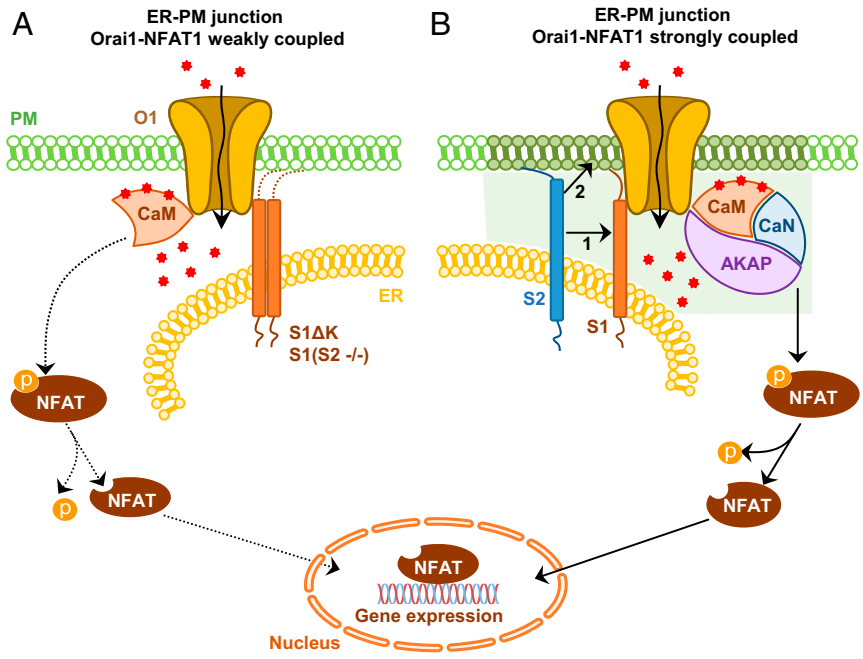

Fig. 6. Model depicting the role of STIM2 in coupling Orai1-mediated Ca^{2+} entry with NFAT1 activation. (*A*) Orai1-mediated SOCE and NFAT1 signaling are weakly coupled in cells expressing Orai1 (O1)+STIM1 (S1) with knockdown of endogenous STIM2 (S2 $^{-/-}$) or Orai1+STIM1ΔK (S1ΔK) despite clustering of Orai1 with STIM1 and a sufficient increase in local $[Ca^{2+}]_i$. (*B*) Assembly of Orai1/STIM1 with STIM2 in ER-PM junctions facilitates strong coupling of Orai1 function with NFAT1 activation. In the presence of STIM2, Orai1 interacts with Ca^{2+}-bound calmodulin (CaM) and the AKAP79 (AKAP)/calcineurin (CaN) complex, allowing local $[Ca^{2+}]_i$ to selectively activate calcineurin, which then dephosphorylates NFAT1 and triggers its translocation to the nucleus. Possible ways in which STIM2 could confer efficient Orai1-NFAT1 signaling are by 1) interacting with and targeting the Orai1/STIM1 complex to ER-PM junctions and 2) changing the organization of ER-PM junctions, which secondarily favors the Orai1-AKAP79 interaction.

DNA Constructs. YFP- and CFP-tagged STIM1/STIM2 constructs were obtained from Tobias Meyer, Stanford University. YFP-STIM2ΔK5 was created as described previously (19). CFP-STIM2ΔSOAR was generated using the method described earlier for YFP-STIM2ΔSOAR (19). mCherry-STIM2 was created using the YFP-STIM2 as a template and replacing the YFP tag with mCherry. The peGFP-N1 vector carrying the HA-mCherry-hSTIM1 was used as PCR template to construct hSTIM1-ΔK with hSTIM2 K-rich domain (mCherry-STIM1-S2K). The 5′-GGC GAG GGC GAG GGC-3′ forward and 5′-TAT AGT CGA CTC ACT TAG ATT TCT TCT TAA AAA GGC TTT TGA TTT TTG ATG GCT TTT TGC TTT TGC CTG GGC TGG AGT CTG TTT C-3′ reverse primers were used to generate a 2,647-bp PCR product. The forward primer annealed 105 nucleotides downstream of the start of the mCherry ORF. At 581 bp downstream of the primer annealing site, the mCherry contained an intrinsic BsrGI restriction site (just before the end of the mCherry ORF). The reverse primer was designed to anneal to the STIM1 region encoding for 664 to 670 residues (just upstream of the polybasic domain) and contained an overhang encoding the STIM2-polybasic domain KSKKPSKIKSLFKKKSK, followed by a stop codon and SalI restriction site.

The PCR product was digested with BsrGI-HF and SalI-HF enzymes (New England BioLabs), and the resulting 2,042-bp digested product (insert) was purified using agarose gel electrophoresis. The peGFP-N1 vector carrying the HA-mCherry-hSTIM1 was also digested with BsrGI-HF and SalI-HF enzymes, and the 4,780-bp vector backbone was purified by agarose gel electrophoresis. The insert and the vector backbone were ligated overnight at 16 °C using T4 DNA ligase (New England BioLabs). The sequence of the final construct was verified by Microsynth, Balgach, Switzerland. Orai1-CFP, YFP-Tubby, and rapamycin-inducible 5′ phosphatase were obtained from Tamas Balla, Eunice Kennedy Shriver National Institute of Child Health and Human Development. mCherry-STIM1 and mCherry-STIM1ΔK were provided by Richard Lewis, Stanford University, and Myc-tagged STIM1 was provided by Shmuel Muallem, National Institute of Dental and Craniofacial Research. The mCherry-ER3 (ER marker), Myc- and GCaMP6f-tagged Orai1, and NFAT1-GFP constructs were obtained from Addgene.

Ca^{2+} Imaging. HEK293 cells were plated on collagen-coated glass coverslips (Neuvitro) and loaded with Fura2-AM. Fura2 fluorescence in cells was measured by ratiometric imaging using an Olympus IX50 microscope, a Polychrome V monochromator (TILL Photonics), and an EM-CCD camera (Hamamatsu). Image acquisition and data processing were done using the MetaFluor imaging system (Molecular Devices). Origin software (OriginLab) was used for data analysis. For SOCE experiments, CPA (25 μM) or Tg (1 μM) was added to cells bathed in medium containing 1 mM $CaCl_2$. For Ca^{2+} addback experiments, CPA or Tg was initially added to cells bathed in Ca^{2+}-free medium, followed by a second addition of 1 mM $CaCl_2$. All additions are indicated by arrows in the graphs.

NFAT Nuclear Translocation. Translocation of NFAT in transfected HEK293 cells was measured (18, 19, 23) using NFAT1-GFP and an Olympus IX50 microscope attached to a Polychrome V monochromator (TILL Photonics) and an EM-CCD camera (Hamamatsu). Image acquisition and data processing were done using MetaFluor and MetaMorph, respectively (Molecular Devices). Origin software (OriginLab) was used for data analysis.

Co-IP and Western Blot Analysis. Cells were transfected and treated as indicated, washed three times with 1× PBS, and lysed in Pierce IP lysis buffer supplemented with protease inhibitors (~8.8×10^6 cells/sample in 700 μL of lysis buffer; all from Thermo Fisher Scientific). Cell lysates were centrifuged at 10,000 × *g* for 10 min at 4 °C and then quantified using Bio-Rad protein assay solution. Part of this lysate was saved for Western blot analysis to indicate control loading. Unless indicated otherwise, co-IP experiments were done using 0.2 to 0.5 mg each of the protein lysates and Protein A Sepharose CL-4B (GE Healthcare Life Sciences) as described previously (18). For Myc-tagged proteins, Pierce anti–c-Myc magnetic beads (Thermo Fisher Scientific) were used in accordance with the manufacturer's instructions. In some cases, a more stringent washing buffer was used to reduce nonspecific binding of the proteins to the beads.

The immunoprecipitants were eluted in gel-loading buffer by heating at 95 °C for 5 to 10 min. Control lysates (25 μg/lane) and eluted immunoprecipitants were resolved in 4 to 12% NuPAGE gels (Life Technologies), followed by Western blotting. Proteins of interest were detected using anti-Orai1 (19), anti-STIM2 (Cell Signaling Technology), anti-AKAP79 (EMD Millipore), or anti–β-actin (Abcam) antibodies. The density of each protein was normalized to its loading control and expressed relative to the condition indicated in the figure legends.

TIRFM Imaging. HEK293 cells were plated on collagen-coated glass-bottom tissue culture dishes (MatTek), transfected as required and used 24 to 48 h later. TIRFM was performed using an Olympus IX81 motorized inverted microscope with a TIRF-optimized Olympus Plan APO 60× (1.45 NA) oil immersion objective and Lambda 10-3 filter wheel (Sutter Instruments) containing 480-bandpass (BP 40 m), 540-bandpass (BP 30 m), and 575lp emission filters (Chroma Technology). Images were collected using a Hamamatsu ORCA-Flash4.0 camera and MetaMorph imaging software (Molecular Devices). Data were analyzed using MetaMorph and Origin (OriginLab) software.

Statistics. Statistical analyses were performed using Origin (OriginLab) and GraphPad Prism (GraphPad Software). Statistical comparisons between two groups were done using Student's *t* test, whereas comparisons of multiple groups were made using ANOVA followed by Sidak's multiple comparisons test. Experimental values are expressed as mean ± SEM.

Data Availability. This article has no additional datasets, code, or materials other than those discussed in the text.

ACKNOWLEDGMENTS. We thank Drs. Richard Lewis, Tamas Balla, Tobias Meyer, and Shmuel Muallem for kindly sharing the various constructs (as specified in *Materials and Methods*). Funding for this work was provided by the National Institute of Dental and Craniofacial Research Division of Intramural Research Grant Z01-DE00438-33 (to I.S.A.) and NIH Grants AI097302 and AI130143 (to S.F.).

1. H. L. Ong, L. B. de Souza, K. T. Cheng, I. S. Ambudkar, Physiological functions and regulation of TRPC channels. *Handb. Exp. Pharmacol.* **223**, 1005–1034 (2014).
2. H. L. Ong, K. P. Subedi, G. Y. Son, X. Liu, I. S. Ambudkar, Tuning store-operated calcium entry to modulate Ca^{2+}-dependent physiological processes. *Biochim. Biophys. Acta Mol. Cell Res.* **1866**, 1037–1045 (2019).
3. O. Brandman, J. Liou, W. S. Park, T. Meyer, STIM2 is a feedback regulator that stabilizes basal cytosolic and endoplasmic reticulum Ca^{2+} levels. *Cell* **131**, 1327–1339 (2007).
4. J. Liou, M. Fivaz, T. Inoue, T. Meyer, Live-cell imaging reveals sequential oligomerization and local plasma membrane targeting of stromal interaction molecule 1 after Ca^{2+} store depletion. *Proc. Natl. Acad. Sci. U.S.A.* **104**, 9301–9306 (2007).
5. M. Prakriya *et al*., Orai1 is an essential pore subunit of the CRAC channel. *Nature* **443**, 230–233 (2006).
6. M. Vig *et al*., CRACM1 multimers form the ion-selective pore of the CRAC channel. *Curr. Biol.* **16**, 2073–2079 (2006).
7. A. V. Yeromin *et al*., Molecular identification of the CRAC channel by altered ion selectivity in a mutant of Orai. *Nature* **443**, 226–229 (2006).
8. P. Kar, D. Bakowski, J. Di Capite, C. Nelson, A. B. Parekh, Different agonists recruit different stromal interaction molecule proteins to support cytoplasmic Ca^{2+} oscillations and gene expression. *Proc. Natl. Acad. Sci. U.S.A.* **109**, 6969–6974 (2012).
9. P. Kar, C. Nelson, A. B. Parekh, Selective activation of the transcription factor NFAT1 by calcium microdomains near Ca^{2+} release-activated Ca^{2+} (CRAC) channels. *J. Biol. Chem.* **286**, 14795–14803 (2011).
10. K. Samanta, P. Kar, G. R. Mirams, A. B. Parekh, Ca^{2+} channel re-localization to plasma-membrane microdomains strengthens activation of Ca^{2+}-dependent nuclear gene expression. *Cell Rep.* **12**, 203–216 (2015).
11. Y. Zhou *et al*., The STIM1-binding site nexus remotely controls Orai1 channel gating. *Nat. Commun.* **7**, 13725 (2016).
12. I. Frischauf *et al*., Transmembrane helix connectivity in Orai1 controls two gates for calcium-dependent transcription. *Sci. Signal.* **10**, eaao0358 (2017).
13. P. Kar *et al*., Dynamic assembly of a membrane signaling complex enables selective activation of NFAT by Orai1. *Curr. Biol.* **24**, 1361–1368 (2014).
14. G. N. Huang *et al*., STIM1 carboxyl-terminus activates native SOC, $I_{(crac)}$ and TRPC1 channels. *Nat. Cell Biol.* **8**, 1003–1010 (2006).
15. C. Y. Park *et al*., STIM1 clusters and activates CRAC channels via direct binding of a cytosolic domain to Orai1. *Cell* **136**, 876–890 (2009).
16. T. Kawasaki, I. Lange, S. Feske, A minimal regulatory domain in the C terminus of STIM1 binds to and activates ORAI1 CRAC channels. *Biochem. Biophys. Res. Commun.* **385**, 49–54 (2009).
17. X. Wang *et al*., Distinct Orai-coupling domains in STIM1 and STIM2 define the Orai-activating site. *Nat. Commun.* **5**, 3183–3193 (2014).
18. H. L. Ong *et al*., STIM2 enhances receptor-stimulated Ca^{2+} signaling by promoting recruitment of STIM1 to the endoplasmic reticulum-plasma membrane junctions. *Sci. Signal.* **8**, ra3 (2015).
19. K. P. Subedi, H. L. Ong, G. Y. Son, X. Liu, I. S. Ambudkar, STIM2 induces activated conformation of STIM1 to control Orai1 function in ER-PM junctions. *Cell Rep.* **23**, 522–534 (2018).
20. M. Oh-Hora *et al*., Dual functions for the endoplasmic reticulum calcium sensors STIM1 and STIM2 in T cell activation and tolerance. *Nat. Immunol.* **9**, 432–443 (2008).
21. S. Song *et al*., STIM2 (stromal interaction molecule 2)-mediated increase in resting cytosolic free Ca^{2+} concentration stimulates PASMC proliferation in pulmonary arterial hypertension. *Hypertension* **71**, 518–529 (2018).
22. Y. Miao *et al*., Calcium-sensing stromal interaction molecule 2 upregulates nuclear factor of activated T cells 1 and transforming growth factor-β signaling to promote breast cancer metastasis. *Breast Cancer Res.* **21**, 99 (2019).
23. H. L. Ong, S. I. Jang, I. S. Ambudkar, Distinct contributions of Orai1 and TRPC1 to agonist-induced $[Ca^{2+}]_i$ signals determine specificity of Ca^{2+}-dependent gene expression. *PLoS One* **7**, e47146 (2012).
24. W. Stauffer, H. Sheng, H. N. Lim, EzColocalization: An ImageJ plugin for visualizing and measuring colocalization in cells and organisms. *Sci. Rep.* **8**, 15764 (2018).
25. E. Ercan, S. H. Chung, R. Bhardwaj, M. Seedorf, Di-arginine signals and the K-rich domain retain the Ca^{2+} sensor STIM1 in the endoplasmic reticulum. *Traffic* **13**, 992–1003 (2012).
26. M. K. Korzeniowski *et al*., Dependence of STIM1/Orai1-mediated calcium entry on plasma membrane phosphoinositides. *J. Biol. Chem.* **284**, 21027–21035 (2009).
27. Z. Szentpetery, A. Balla, Y. J. Kim, M. A. Lemmon, T. Balla, Live cell imaging with protein domains capable of recognizing phosphatidylinositol 4,5-bisphosphate; a comparative study. *BMC Cell Biol.* **10**, 67 (2009).
28. P. Kar, C. Nelson, A. B. Parekh, CRAC channels drive digital activation and provide analog control and synergy to Ca^{2+}-dependent gene regulation. *Curr. Biol.* **22**, 242–247 (2012).
29. J. L. Dynes, A. Amcheslavsky, M. D. Cahalan, Genetically targeted single-channel optical recording reveals multiple Orai1 gating states and oscillations in calcium influx. *Proc. Natl. Acad. Sci. U.S.A.* **113**, 440–445 (2016).
30. S. F. Oliveria, M. L. Dell'Acqua, W. A. Sather, AKAP79/150 anchoring of calcineurin controls neuronal L-type Ca^{2+} channel activity and nuclear signaling. *Neuron* **55**, 261–275 (2007).
31. X. Zhang *et al*., A calcium/cAMP signaling loop at the ORAI1 mouth drives channel inactivation to shape NFAT induction. *Nat. Commun.* **10**, 1971 (2019).
32. R. Bhardwaj, H. M. Müller, W. Nickel, M. Seedorf, Oligomerization and Ca^{2+}/calmodulin control binding of the ER Ca^{2+} sensors STIM1 and STIM2 to plasma membrane lipids. *Biosci. Rep.* **33**, e00077 (2013).
33. S. Dai, D. D. Hall, J. W. Hell, Supramolecular assemblies and localized regulation of voltage-gated ion channels. *Physiol. Rev.* **89**, 411–452 (2009).
34. Y. Guo *et al*., AKAP5 signaling complexes: Focal points and functional properties. *Neuroendocrinol. Lett.* **36**, 7–14 (2015).
35. C. J. Penny, M. G. Gold, Mechanisms for localising calcineurin and CaMKII in dendritic spines. *Cell. Signal.* **49**, 46–58 (2018).
36. J. Zhang, M. S. Shapiro, Mechanisms and dynamics of AKAP79/150-orchestrated multiprotein signalling complexes in brain and peripheral nerve. *J. Physiol.* **594**, 31–37 (2016).
37. D. Willoughby *et al*., A key phosphorylation site in AC8 mediates regulation of Ca^{2+}-dependent cAMP dynamics by an AC8-AKAP79-PKA signalling complex. *J. Cell Sci.* **125**, 5850–5859 (2012).
38. D. Willoughby *et al*., Direct binding between Orai1 and AC8 mediates dynamic interplay between Ca^{2+} and cAMP signaling. *Sci. Signal.* **5**, ra29 (2012).